Applied Catalysis B: Environmental 259 (2019) 118093

Contents lists available at ScienceDirect

Applied Catalysis B: Environmental

journal homepage: www.elsevier.com/locate/apcatb

A core-shell SO_4/Mg-Al-Fe_3O_4 catalyst for biodiesel production

Jabbar Gardy[a], Ehsan Nourafkan[b], Amin Osatiashtiani[c], Adam F. Lee[d], Karen Wilson[d], Ali Hassanpour[a,*], Xiaojun Lai[a,*]

[a] School of Chemical and Process Engineering, University of Leeds, West Yorkshire, Leeds, LS2 9JT, UK
[b] School of Mathematics and Physics, University of Lincoln, Lincolnshire, Lincoln, LN6 7TS, UK
[c] European Bioenergy Research Institute, Aston University, Aston Triangle, Birmingham, B4 7ET, UK
[d] Applied Chemistry and Environmental Science, RMIT University, Melbourne, VIC 3000, Australia

ARTICLE INFO

Keywords:
Solid acid catalyst
Magnetic catalyst
Core-shell nanoparticle
Waste cooking oil
Biodiesel

ABSTRACT

Catalytic transesterification of triglycerides and esterification of free fatty acids underpins sustainable biodiesel production, wherein efficient heterogeneous catalysts are sought to replace mineral acids. A robust, magnetic core-shell SO_4/Mg-Al-Fe_3O_4 catalyst was synthesised by stepwise co-precipitation, encapsulation, and surface functionalisation. The resulting magnetically-separable catalyst has a surface area of 123 $m^2 g^{-1}$, uniform 6.5 nm mesopores, and a high total acid site loading of 2.35 mmol g^{-1}. Optimum conditions for the (trans) esterification of waste cooking oil (WCO) over the sulfated solid acid catalyst were 95 °C, a methanol:WCO molar ratio of 9:1, and 300 min reaction to achieve 98.5% FAME yield. Esterification of oleic acid to methyl oleate resulted in an 88% yield after 150 min under the same reaction conditions. The magnetic solid acid catalyst exhibited good thermal and chemical stability and enabled facile catalyst separation post-reaction and the production of high quality biodiesel.

1. Introduction

Energy is a key driving force for transportation, technological advancement, and industrialisation and underpins global socioeconomic development [1–3]. Biodiesel, comprising fatty acid methyl esters (FAME), is widely recognised as a potential low carbon alternative to fossil fuel derived diesel [4], owing to its low toxicity, eco-friendliness [5,6] and sourcing from non-edible plant and algal oils and animal fats [7–9]. Oils from (micro)algae, jatropha seeds, and waste cooking oil (WCO) feedstocks have been used to reduce biodiesel production costs [9–14]. For example, the amount of WCO generated in the United Kingdom is estimated at 65,000 to 80,000 tons per annum while in China this figure reaches 1,000,000 to 2,500,000 per annum from commercial and food processing industries [15]. Such sources could provide an economic alternative to virgin plant oils for biodiesel production, and valorise an otherwise problematic waste stream [2]. However, untreated WCO contains high amounts of free fatty acids (FFAs) and water which renders it an unsuitable feedstock for homogenous base catalysed transesterification with alkaline hydroxides and methoxides due to catalyst neutralisation, hydrolysis of the FAME product, and saponification and attendant separation issues due to the formation of stable emulsions. Homogeneous (acid or base) catalysts also generate large quantities of contaminated wastewater during biodiesel neutralisation [13,16–19], and essential processing step to avoid engine corrosion.

Solid acids and bases can offer good catalytic activity under mild conditions for the (trans)esterification processes of WCO feedstocks [18], and enable efficient product separation and catalyst recycling, in addition to continuous biodiesel production [20]. Although base catalysts are generally more active for triacylglyceride (TAG) transesterification, their sensitivity to FFA contaminants (and necessity for feedstock pre-treatment to remove such impurities) remain problematic [21]. Solid acid catalysts are more resistant to high FFA concentrations, and can simultaneously transesterify TAGs and esterify FFAs to biodiesel [22,23]. The catalytic activity of solid acids is strongly dependent on the accessibility of bulky reactants to active sites, and the number, strength, and type (Brønsted and/or Lewis) of active site. Numerous solid acids have been explored for biodiesel production, including zeolites, metal oxides and mixed metal oxides, supported acids, polyoxometallates, sulfonated carbons, cation exchange resins and sulfated metal oxides [13,18,21,24–26]. Sulfated metal oxides have attracted significant interest in catalysis [23,27–32], and are typically synthesised by the preparation of metal oxide sol gel (step 1), the subsequent introduction of sulfate ions by exposure of the sol gel to sulfuric acid

* Corresponding authors.
E-mail addresses: A.Hassanpour@leeds.ac.uk (A. Hassanpour), X.Lai@leeds.ac.uk (X. Lai).

https://doi.org/10.1016/j.apcatb.2019.118093
Received 19 December 2018; Received in revised form 12 May 2019; Accepted 13 August 2019
Available online 16 August 2019

[H_2SO_4], chlorosulfonic acid [HSO_3Cl], or ammonium sulfate [$(NH_4)_2SO_4$] (step 2), and a final calcination at high temperature (step 3). The resulting solid superacidic features SO_4^{2-} groups at the surface on non-porous metal oxide nanoparticles. The acidity of sulfated metal oxides depend on the degree of hydration, preparation method and calcination temperature of the sulfated metal oxide, and the sulfate concentration and presence of neighbouring strong Lewis acid sites [33,34]. Low sulfate loadings promote bidentate adsorption geometries, whereas high loadings favour Brønsted acidic polynuclear (pyro)sulfates [35,36]. Sulfated metal oxides, binary metal oxides, and ternary metal oxides are all reported as promising solid acid catalysts for biodiesel production from low cost feedstocks in the presence of FFAs, water, and other impurities. Studies from several authors [37–43] showed that the catalytic activity of sulphated metal oxides could be improved by their fast separation from the product and by-products. The magnetic catalyst has the potential to overcome the limitation for separating solid acid catalysts from the reaction medium. Furthermore, the acidity of magnetic solid acid catalyst reported to be stronger ($H_0 < -13.8$) than 100% sulfuric acid ($H_0 = -12$). For example, the uniform and monodispersed iron oxide nanoparticles were designed by co-precipitation method followed by growing zirconia on the surface of iron oxide nanoparticles whilst the introduction of boron oxide into the solution was to inhibit the nucleation and grain growth of zirconia by delaying the phase transformation of zirconia from tetragonal to monoclinic. The catalytic activity was tested at different calcination temperatures (400–900 °C) for esterifying acetic acid with n-butanol. A yield of 97 ± 1% was reported under optimum conditions of 4 h, 100 °C, 850 RPM, and 1 atm nitrogen pressure [39]. Another recent study by Wu and co-workers [38] reports the design of a super paramagnetic polysulphated trinary metal oxides catalyst for the transesterification of cottonseeds with methyl acetate. The core was made from iron oxide and prepared by co-precipitation method. Titania and zirconia was introduced to the iron oxide core by another co-precipitation with different mole ratios of Zr/Ti/Fe, followed by impregnation of sulphate ions from $(NH_4)_2S_2O_8$. The final gel was calcined at 550, 650 and 750 °C for 3 h. The synthesised magnetic catalysts showed super acidity (155.3 ± 0.9–598.6 ± 1.3 μmol/g) with polysulphate ions coordinated to ZrO_2-TiO_2-Fe_3O_4 catalyst support. It was reported that SO_4/ZrO_2-TiO_2-Fe_3O_4 catalyst calcined at 550 °C enabling a FAME yield of 99% after 10.8 h at 50 °C with 21.3 wt% of catalyst and 13.8 ml of methyl acetate per g of seed. The acidity of the catalyst increased with the addition of an appreciable amount of titania (3:1 mol ratio of Zr:Ti) into the catalyst texture due to the formation of Zr-O-Ti units during the calcination. This resulted in more sulphur species being adsorbed on the surface and inhibit the zirconia grain growth. As a result, the number of Lewis acid sites increased which enhanced the catalytic activity of the catalyst. The catalyst was re-used for 8 cycles with a slight decrease in activity. Alhassan et al. [37] have also designed a bifunctional magnetic sulphated ternary metal oxide [Fe_2O_3-MnO-SO_4/ZrO_2] catalyst via impregnation method followed by calcination at 600 °C for 3 h. This magnetic catalyst was tested for transesterification of WCO under optimum conditions of 180 °C reaction temperature, 20:1 mol ratio of methanol to oil, 3 wt% of catalyst loading, and 600 RPM stirring rate, where 97 ± 0.5% of FAME yield was obtained. The loss of catalytic activity reported after 6 re-runs of the spent catalyst because of pore blockage and sulphur leaching. In summary, the catalytic activity of sulphated metal oxide depends mainly on the precursors, type of sulfonating agent, calcination temperature, amount of sulphate content, and crystallinity of the catalyst. However, there are still prone to deactivation, active site leaching, mass transport limitations, low activity at lower temperatures, water sensitivity, low surface area, and difficult and/or time-consuming separation by filtration or centrifugation [10,38,44–49]. These drawbacks highlight the continuing need to design improved catalysts for esterification and transesterification of WCO. Here we report the preparation of a magnetic core-shell SO_4/Mg-Al-Fe_3O_4 nanocatalyst for the simultaneous esterification and transesterification of WCO with methanol under mild conditions. The Fe_3O_4 core facilitates magnetic separation of the solid acid catalyst from the reaction media, while the encapsulating $MgAlO_x$ shell protects the magnetic core and increases the nanoparticle surface area prior to sulfation conferring good activity and stability for biodiesel production even in the presence of high FFA concentrations.

2. Experimental

2.1. Synthesis of magnetic core-shell SO_4/Mg-Al-Fe_3O_4 catalyst

Iron oxide nanoparticles were synthesised by co-precipitation ($Fe^{2+} + 2\ Fe^{3+} + 8\ OH^- \rightarrow Fe_3O_4 + 4\ H_2O$). 0.2 mol $FeCl_2.4H_2O$, (≥99.99%, Sigma-Aldrich) and 0.68 mol $FeCl_3.6H_2O$ (≥98%, Sigma-Aldrich) were separately dissolved in 25 ml of an aqueous 1:1 vol% ethanol (≥99.8%, Sigma-Aldrich) solution using an ultrasonic probe. The resulting clear solutions were added to a 250 ml round-bottomed flask, and the solution pH held at 12 by dropwise addition of NH_4OH (28–30 vol%, Sigma-Aldrich), prior to heating at 80 °C during stirring (250 rpm) for 6 h under a N_2 atmosphere. Following 24 h ageing at room temperature, iron oxide nanoparticles were isolated using an external magnetic field (Nd magnet), and repeatedly rinsed with 1:1 vol % aqueous ethanol until chloride ions could not be detected in the washings. The resulting dark-reddish particles were dried in an oven at 120 °C overnight, and then calcined at 550 °C for 3 h to obtain Fe_3O_4 nanoparticles.

Magnesium oxide and alumina encapsulated Fe_3O_4 nanoparticles were synthesised as follows: 3 g of as-prepared Fe_3O_4 nanoparticles were dispersed in 50 ml of 1:1 vol% aqueous isopropanol (+99.5%, Sigma-Aldrich) using an ultrasonic probe. Subsequently, 50 ml of 1:1 vol% aqueous IPA, 0.6 mol $Al(O\text{-}i\text{-}Pr)_3$ (+98% granular, Alfa Aesar) and 0.25 mol $Mg(NO_3)_2.6H_2O$ (≥99.9%, Sigma-Aldrich) were added dropwise to the mixture along with 1.5 ml of HNO_3 (≥90.0%, Sigma-Aldrich). The resulting solution was mixed at room temperature for 30 min, and the pH then adjusted to 7 using NH_4OH. This slurry was held at 65 °C during stirring at 250 rpm for 4 h, and then aged at room temperature overnight, and the encapsulated $MgO@Al_2O_3@Fe_3O_4$ particles magnetically separated, washed with deionised water until pH neutral, and then dried in an oven at 80 °C for 6 h before a final calcined at 550 °C for 2 h. The preceding nanoparticles were functionalised by sulfation. 1.0 g of as-prepared $MgO@Al_2O_3@Fe_3O_4$ nanoparticles was added to 10 ml of 0.5 M $(NH_4)_2SO_4$ (≥99.5%, VWR International Ltd) aqueous solution and stirred for 6 h at room temperature. The sulfated nanoparticles were magnetically separated, dried in an oven at 80 °C for 6 h, and finally calcined at 500 °C for 3 h in static air. This sample is denoted SO_4/Mg-Al-Fe_3O_4.

2.2. Catalyst characterisation

Powder XRD patterns were measured using a Bruker D8 diffractometer with Cu K_α (λ = 1.5418 Å) radiation and a LynxEye detector between 10-70° with steps of 0.035° at 5 s per step. Particle morphology, and elemental composition and spatial distributions were determined using a Hitachi SU8230 cold field emission scanning electron microscope (SEM) operated at 2 kV, and FEI Titan Themis Cubed 300 transmission electron microscope (TEM) coupled with an Oxford INCA energy dispersive X-ray spectrometer (EDS). For the TEM analysis magnetic nanoparticles were dispersed in acetone and then drop cast on a carbon coated copper grid. Surface functional groups were examined at room temperature using a Nicolet iS10 FTIR spectrometer by attenuated total reflectance (ATR) between 550–4000 cm^{-1} at a resolution of 4 cm^{-1}. Textural properties were obtained by N_2 physisorption method at 77 K using a Micromeritics TriStar 3000 porosimeter. The as-prepared magnetic catalyst was degassed in vacuo at 120 °C for 16 h prior to analysis, and the surface area calculated using the Brunauer–Emmett–Teller (BET) method over the relative pressure (p/

p_0) range 0.05-0.2, with pore size distributions determined by the Barrett-Joyner-Halenda (BJH) method applied to the desorption isotherm. Thermogravimetric analysis (TGA) was performed using a Mettler Toledo TGA/DSC-2 instrument under N_2 gas at 50 ml min^{-1} and a heating rate of 10 °C min^{-1} from 25 to 900 °C. Total sulfate loadings were determined from the mass loss by TGA between 600–900 °C and using a Thermo Scientific™ FLASH 2000 CHNS-O elemental analyser. Metal loadings were determined using a PerkinElmer Sciex inductively coupled plasma-mass spectroscopy (ICP-MS). Acid site loadings were quantified by n-propylamine chemisorption and subsequent temperature programmed desorption (TPD) under flowing He at 30 ml min^{-1} and a heating rate of 10 °C min^{-1} from 40 to 800 °C. The catalyst was first saturated with n-propylamine (Sigma-Aldrich, ≥ 99.0% GC grade), and physisorbed species removed by in vacuo drying at 30 °C overnight [5]. Thermal desorption of reactively-formed propene (m/z = 41) and ammonia (m/z = 17) from propylamine decomposition was monitored using a Pfeiffer ThermoStar quadupole mass spectrometer.

2.3. Catalyst testing

2.3.1. Esterification and transesterification of WCO

WCO was obtained from a restaurant in Leeds, and contained 0.14 wt% moisture and 2 wt% FFA [5]. Transesterification and esterification was conducted in a stirred glass batch reactor connected to a Ministat Huber 125 Pilot ONE temperature controller and reflux condenser. The WCO was pre-treated by simple filtration to remove physical impurities, and then heated to 100 °C to remove water. Physicochemical properties of the waste cooking oil were measured after this pre-treatment. Pre-treated WCO was mixed with methanol (≥99.9%, HPLC grade Sigma-Aldrich) to achieve the desired molar ratio and added to the glass reactor at room temperature, together with the desired mass of SO_4/Mg-Al-Fe_3O_4 catalyst. The reaction mixture was then stirred at 600 rpm and heated to the required temperature. Aliquots of the mixture were periodically sampled for off-line GC–MS analysis using a Perkin Elmer Clarus 580S gas chromatograph, equipped with an Elite 5 ms capillary column (30.0 m x 250 µm) and a 560S mass spectrometer [45].

2.3.2. Esterification of oleic acid

The stability of SO_4/Mg-Al-Fe_3O_4 catalyst was assessed during oleic acid esterification as a model FFA using the optimised process parameters for biodiesel production from WCO. 4.0 wt% of SO_4/Mg-Al-Fe_3O_4 catalyst and 9:1 M ratio of methanol: oleic acid (Fluka Analytical, ≥99.0%) were charged into the glass reactor at room temperature. The three-phase mixture (solid-liquid-liquid) was agitated at 600 RPM and heated to 95 °C. Methyl oleate formation was periodically monitored by withdrawing sample aliquots and off-line GC–MS analysis [45].

2.4. Biodiesel characterisation

A Setaflash series 3 closed cup automated flash point tester was used to capture the flash point of the synthetic biodiesel under a temperature ramp of 1–2 °C min^{-1}. The biodiesel density was calculated using a pycnometric method at 15 °C, and kinematic viscosity measured at 40 °C by a Malvern Bohlin-Gemini 150 rotary rheometer. Acid values and FFA% of the synthetic biodiesel were measured according to standard methods [5]. Free glycerol, mono-, di-, triglyceride and total glycerine contents were quantified using a Perkin Elmer Clarus 560 GC equipped with an on-column injection system, a flame ionization detector and a capillary column (15.0 m x 0.32 mm, 0.1 µm) [50,51]. The total FAME (biodiesel) yield was determined by off-line GC–MS using a modified EN-14103 procedure as previously reported [45] from Eq. 1:

$$\text{Total FAME}\,\% = \frac{(\sum A) - A_{IS}}{A_{IS}} * \frac{C_{IS} * V_{IS}}{W} * 100 \quad (1)$$

where ΣA = total peak area of methyl esters, A_{IS} = peak area of methyl heptadecanoate, C_{IS} = methyl heptadecanoate concentration in mg/ml, V_{IS} = used volume of methyl heptadecanoate solution in ml, and W = sample mass in mg.

2.5. Catalyst reusability and leaching

Catalyst reusability for biodiesel production from WCO was assessed by magnetically separating the post-reaction catalyst from the reaction mixture, washing the catalyst repeatedly with a 1:1 vol% methanol:n-hexane mixture to remove any weakly bound organic residues, and then a final 250 °C re-calcination for 2 h to remove any chemisorbed organics, moisture or CO_2 on the catalyst surface. Leaching from the SO_4/Mg-Al-Fe_3O_4 catalyst was investigated by ICP-MS. A sample of the synthetic biodiesel was digested after each reaction using a HF100-multiwave 3000 (Anton Paar) microwave digester using 7.0 ml of concentrated nitric acid (≥69%, Fluka Analytical, TraceSELECT®), 1.0 ml of concentrated fuming hydrochloric acid (≥37%, Fluka Analytical, TraceSELECT®) and 2.0 ml of hydrogen peroxide (~30%, Sigma-Aldrich, for ultra-trace analysis) reagents. The resulting solutions were diluted with deionised water to 50 ml and then nebulised into the ICP. Mg, S, Al, and Fe concentrations were determined by standard methods [50].

3. Results and discussion

3.1. Catalyst characterisation

Powder XRD of the as-prepared SO_4/Mg-Al-Fe_3O_4 (Fig. 1a) revealed sharp reflections at 18.3, 30.2, 35.5, 37.2, 43.2, 53.6, 57.1, and 62.7°, assigned to the [111], [220], [311], [222], [400], [422], [511] and [440] planes of cubic Fe_3O_4 (magnetite, ICDD: 04-002-3668)

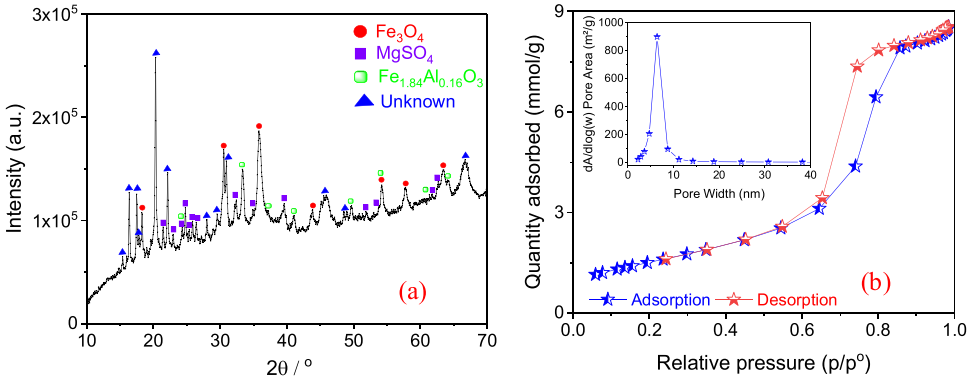

Fig. 1. (a) Powder XRD pattern, and (b) N_2 adsorption-desorption isotherms and mean pore sizes (inset) of as-prepared SO_4/Mg-Al-Fe_3O_4.

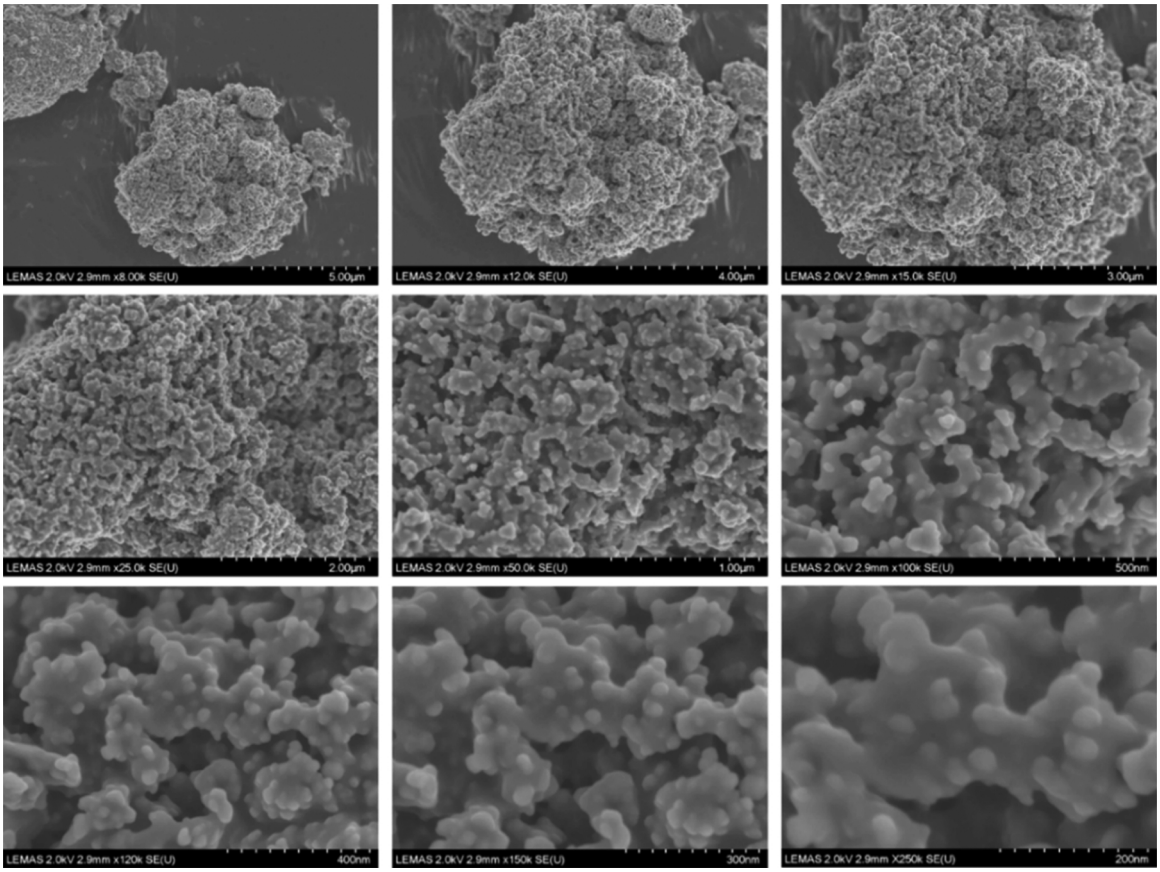

Fig. 2. SEM images at different magnifications for SO_4/Mg-Al-Fe_3O_4 catalyst.

respectively. Particle size analysis applying the Scherrer equation to peak widths indicates volume-averaged Fe_3O_4 crystalline diameters of 86 nm. Reflections were also observed at 24.3, 33.4, 35.8, 41.1, 49.7, 54.4, 62.8, and 64.4° assigned to the [012], [104], [110], [113], [024], [116], [214] and [300] planes respectively of rhombohedral $Fe_{1.84}Al_{0.16}O_3$ (iron aluminium oxide, ICDD: 04-005-8669). Weak reflections are also present between 2θ = 20-65°, attributed to orthorhombic magnesium sulfate ($MgSO_4$, ICDD: 00-021-0546) with cell parameters a = 4.75, b = 8.59 and c = 6.71 Å.

Porosimetry of SO_4/Mg-Al-Fe_3O_4 showed a Type IV isotherm (Fig. 1b) and type H1 hysteresis loop [52] which are typically associated with capillary condensation within cylindrical mesopores. Since the synthesis did not employ a structure-directing template, these mesopores may arise from interparticle voids, but in any even could serve to improve reactant accessibility to active sites. SEM images of the SO_4/Mg-Al-Fe_3O_4 catalyst reveal the formation of large (˜20-40 nm) nanoparticle aggregates (Fig. 2) which are embedded in a (presumably amorphous alumina and/or $MgSO_4$) matrix to form a coral-like porous architecture. TEM images confirm the presence of (high contrast) Fe_3O_4 cores between 20–150 nm diameter, encapsulated by amorphous shells comprising low contrast aggregates of (presumably Al/Mg-rich) of ˜5–15 nm nanoparticles (Fig. 3). Elemental maps confirm that Fe_3O_4 nanoparticles are embedded within an Al-rich matrix (Fig. 4), with Mg co-located with S in a 1:1 atomic ratio. The atomic ratio of Al:Mg = 6:1 throughout the sample which may suppress nucleation and growth of Mg-Al hydrotalcites (unstable for values > 4:1), whereas that for Fe:Mg = 3:1 [53]. The low magnesium content of the as-prepared catalyst may also reflect the low pH used during its synthesis. The total sulfur content determined by TEM-EDS, CHNS-O, and ICP-MS was approximately 7 wt% (Table 1), higher than that reported for SO_4/MO_x (2–3 wt%) [54] and Al-doped SO_4/ZrO_2 (1.5 wt%) [55], but comparable to SO_4/Fe-Al-TiO_2 [5].

The ATR-IR spectrum of SO_4/Mg-Al-Fe_3O_4 exhibited a strong broad band at 3252 cm^{-1} attributed to the O—H stretch of physisorbed water (Fig. 5a) on the surface of the catalyst from the air and/or interlayer water molecules while the peak at 3072 cm^{-1} corresponded to the O—H stretching vibration of bound water [5,38,56]. The strong bands between 982-1087 cm^{-1} are assigned to chelating bidentate sulfate (SO_4^{2-}) and/or chelating double-bridge peroxydisulfate ($S_2O_8^{2-}$) groups, and that at 1418 cm^{-1} to an S═O stretch [38,39]. Bands at 719, 604, and 566 cm^{-1} likely arise from to M—OM— stretches involving Al-O, Mg-O and Fe-O bonds [38,56–59].

TGA of the as-prepared SO_4/Mg-Al-Fe_3O_4 exhibited two distinct weight losses (Fig. 5b). The first, between 100 and 150 °C, is associated with the loss of physisorbed water [60], and the second between 600–900 °C is due to the decomposition of sulfate and/or peroxydisulfate groups and SO_x evolution [5]; sulfate species are thermally stable < 600 °C, superior to that observed for other sulfated metal oxides [39,61]. The sulfate loading calculated from TGA of 11 wt% is in good agreement with elemental analysis. Acid loading and strength of the as-prepared catalyst were quantified by n-propylamine TPD-MS (Fig. 6). A strong desorption peak for reactively-formed propene is observed between 300–500 °C (arising from Hofmann elimination of chemisorbed n-propylamine over acid sites) indicative of moderate strength acid sites akin to those reported in SO_4/ZrO_2 [32]. The calculated total acidic site loadings of the SO_4/Mg-Al-Fe_3O_4 catalyst were found to be 2.35 mmol g^{-1} which is much higher than that reported for other sulfated metal oxides (typically < 1 mmol g^{-1}) [5,62,63].

3.2. Catalytic performance

The as-prepared SO_4/Mg-Al-Fe_3O_4 catalyst was subsequently evaluated for biodiesel production from WCO (Fig. 7). First, the effect of methanol:WCO molar ratio was explored between 3:1 to 12:1;

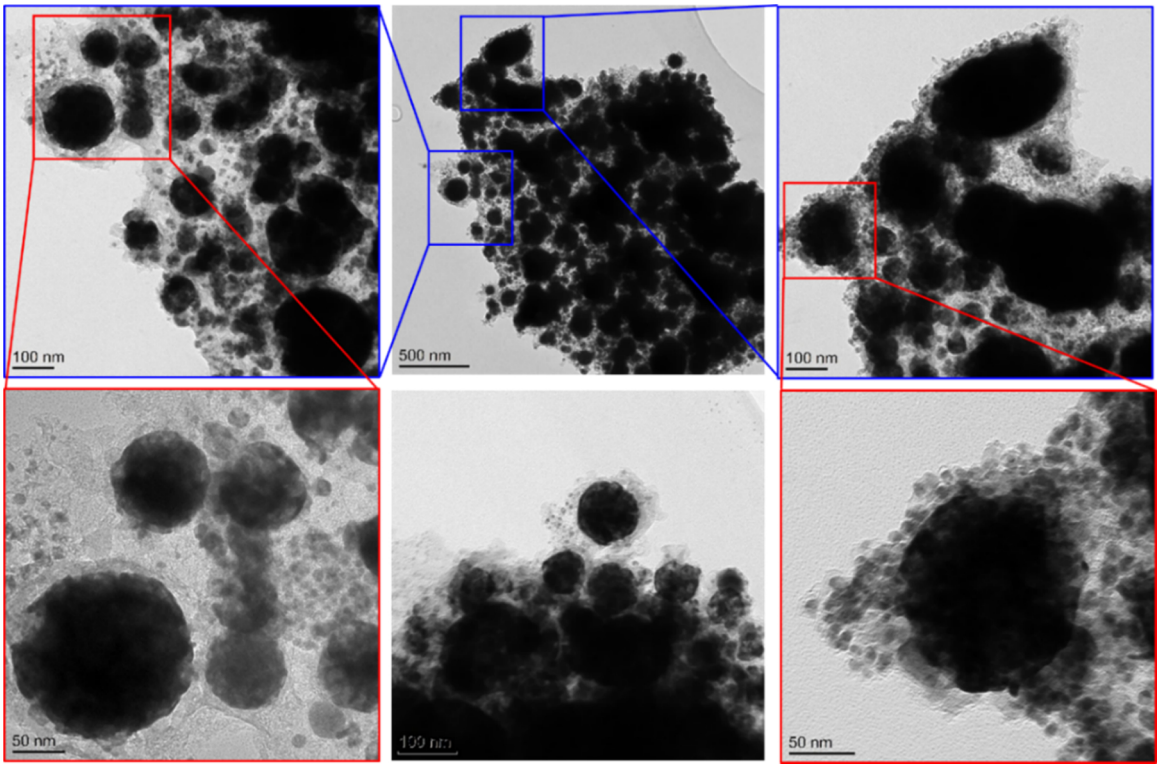

Fig. 3. TEM images of SO_4/Mg-Al-Fe_3O_4 catalyst.

increasing the methanol content monotonically enhanced the 6 h FAME yield from approximately 55 to 80% by shifting the transesterification reaction equilibrium (Fig. 7a). Since only a small yield enhancement was observed for methanol:WCO ratios > 9:1, this reaction composition was employed for all further experiments. Increasing the catalyst mass (with respect to WCO) from 1 to 5 wt% linearly improved the initial FAME yield (Fig. 7b), indicating that transesterification was free from mass-transport limitations during the first hour of reaction reflecting the rise in active sites preceding a slow deactivation at longer reaction times [64]. Final 6 h FAME yields spanned 65–80%. A catalyst loading of 3 wt% was selected as this provided a sufficient yield to measure accurately, while offering scope for improvements during further optimisation without encountering diffusion limitations. The impact of reaction temperatures was also studied between 65 to 95 °C (Fig. 7c) [45]. A significant yield increase was observed on raising the reaction temperature to 75 °C (followed by a more gradual rise at higher temperature) which may both reflect both enhanced rates of TAG hydrolysis and better miscibility of the methanol/WCO liquid phases, as previously reported [65,66]. The maximum 6 h FAME yield > 95% at the highest temperature. To establish the catalyst tolerance to FFAs, oleic acid esterification with methanol was also examined under the optimum reaction conditions (Fig. 7d). SO_4/Mg-Al-Fe_3O_4 catalyst was active for methyl oleate production, with a maximum FAME yield of 87% after 2 h reaction; the small drop in FAME yield at longer reaction times may be associated with water (by-product) accumulation driving the reverse hydrolysis.

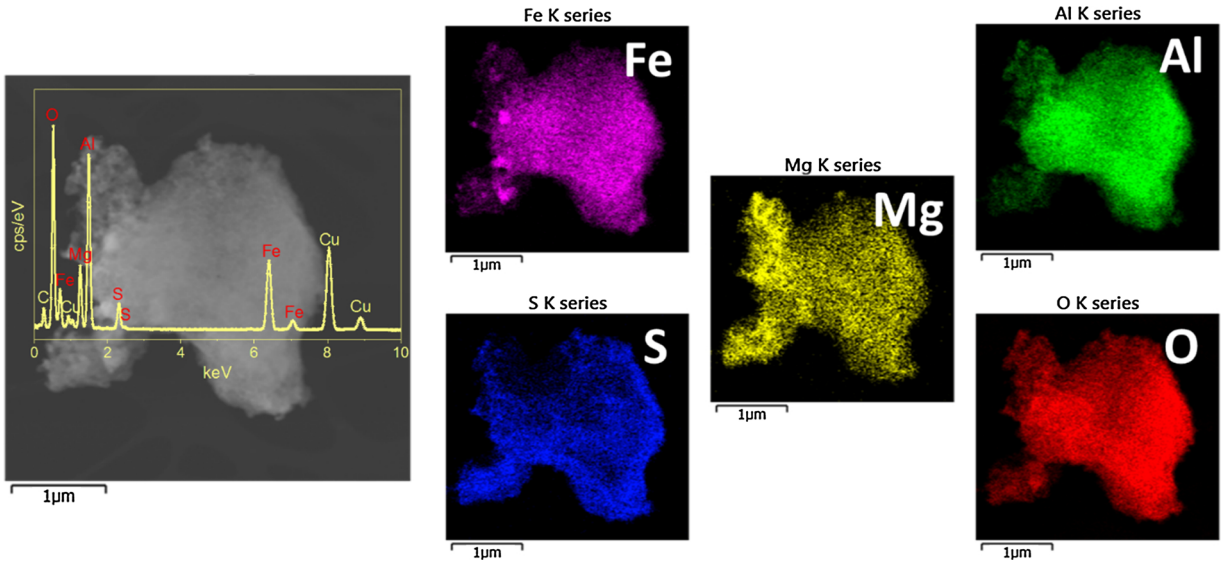

Fig. 4. EDS elemental mapping of SO_4/Mg-Al-Fe_3O_4 catalyst.

Table 1
Textural properties and composition of SO_4/Mg-Al-Fe_3O_4.

	Textural properties[a]			Composition / atom%[b]					Bulk S content/ wt%	
	S_{BET} / $m^2\,g^{-1}$	D_p / nm	V_p / $cm^3\,g^{-1}$	O	Mg	Al	S	Fe		
SO_4/Mg-Al-Fe_3O_4	123 ± 1	6.5 ± 0.5	0.3	60.5	3.5	20.7	4.6	10.7	7.8 ± 1[c]	7.6 ± 0.5[d]

[a] N_2 porosimetry.
[b] EDS.
[c] CHNS-O.
[d] ICP-MS.

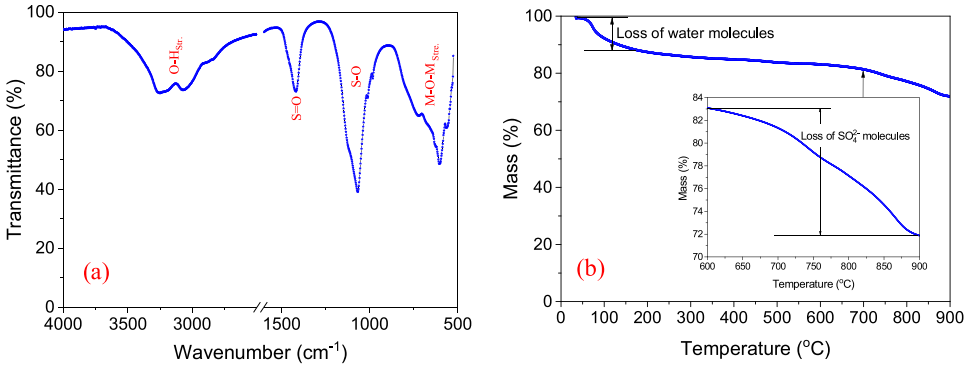

Fig. 5. (a) FTIR spectrum and (b) TGA profile of SO_4/Mg-Al-Fe_3O_4.

3.3. Magnetic catalyst reusability and leaching

Stability of SO_4/Mg-Al-Fe_3O_4 for WCO transesterification was investigated during five catalyst re-uses under optimal reaction conditions (Fig. 8). Minimal deactivation was observed, consistent with post-reaction XRD analysis of the catalyst which evidenced negligible change in the phase or crystallinity, and elemental analysis which revealed negligible metal or sulfur leaching occurred into the reaction medium (Table 2). A small increase in the residual Al and Fe concentrations in the biodiesel product was observed for Run 3, attributed to the use of a different strength magnet to separate the nanoparticles compared with the other four runs. This excellent stability is an important consideration for commercial (large scale) biodiesel production from low grade oil feedstocks.

3.4. Biodiesel characterisation

Analysis of the transesterification biodiesel product is critical to determining the quality of any ultimate fuel blend due to the potential presence of contaminants including glycerol, FFAs, catalyst residue, methanol, and water. GC–MS analysis (Fig. 9) of the biodiesel product was therefore conducted to quantify the biodiesel purity, using a response factor from the methyl heptanoate internal standard (≥ 99.5 % purity, Sigma-Aldrich) to calculate the amount of individual FAME components (Table 3). The major FAME products were methyl palmitate, methyl stearate, methyl oleate, methyl linoleate, methyl linoleate, and methyl gadoleate. The physicochemical properties of the biodiesel confirm that its quality meets ASTM and EU standards (Table 4).

4. Conclusions

A novel magnetically separable SO_4/Mg-Al-Fe_3O_4 core-shell catalyst was synthesised for the transesterification of WCO and esterification of oleic acid. Bulks and surface physicochemical properties were characterised by XRD, SEM, TEM, TGA, ATR-FTIR, N_2 porosimetry, and propylamine TPD-MS. Magnetic Fe_3O_4 (20–150 nm dimeter) nanoparticles were encapsulated by 5–15 nm thick alumina and/or $MgSO_4$ shells. Sulfation generated surface bidentate sulfate ions which exhibited moderate acid strengths but high acid site loadings of 2.35 mmol g^{-1}. The multifunctional catalyst properties (super acidity

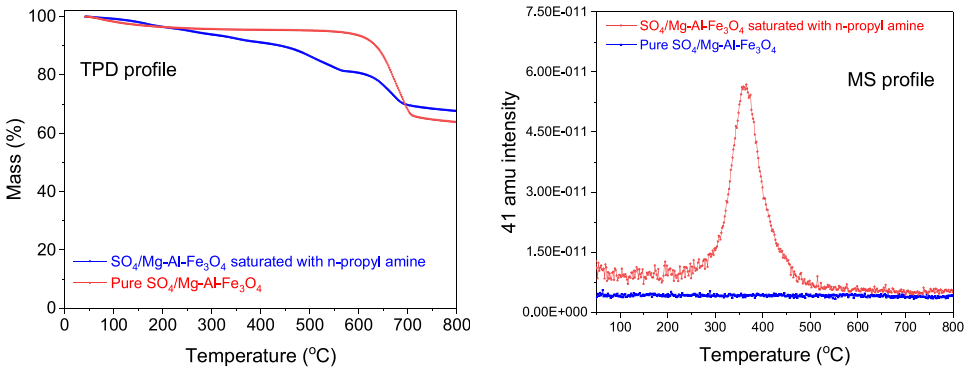

Fig. 6. (left) TPD profiles, and (right) mass spectra for SO_4/Mg-Al-Fe_3O_4 catalyst of pure and saturated with n-propylamine.

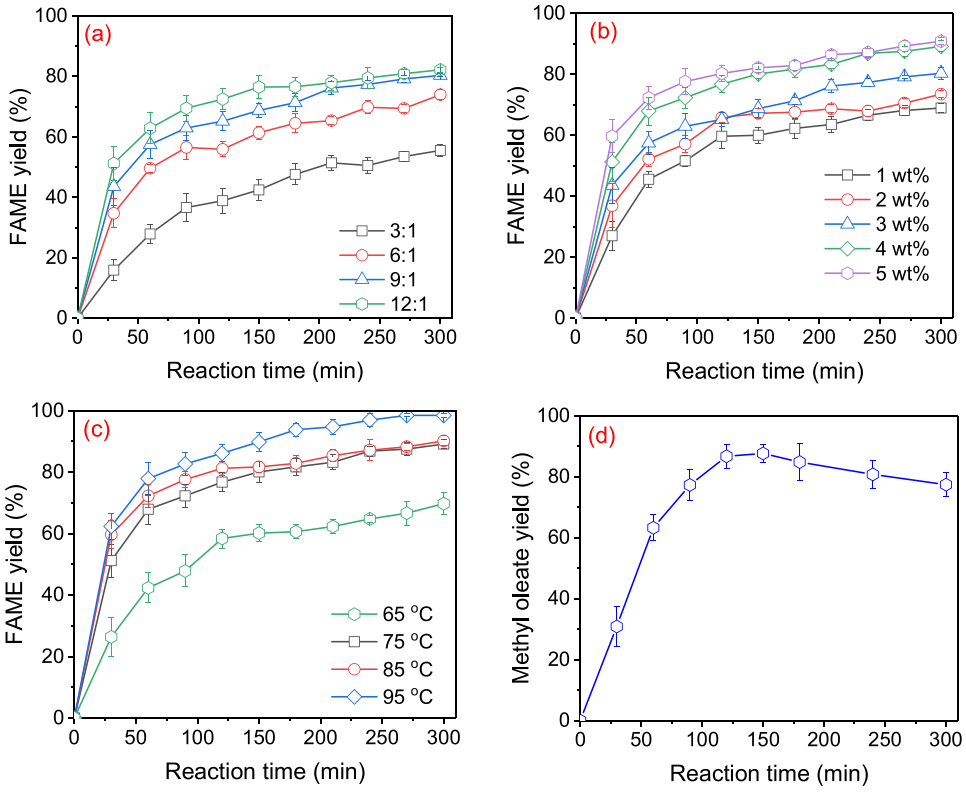

Fig. 7. WCO transesterification over SO_4/Mg-Al-Fe_3O_4 as a function of (a) methanol:WCO molar ratio at 75 °C and 3 wt% catalyst, (b) catalyst loading at 75 °C and 9:1 methanol:WCO molar ratio, and (c) reaction temperature at 4 wt% catalyst and 9:1 methanol:WCO molar ratio. (d) Oleic acid esterification over SO_4/Mg-Al-Fe_3O_4 at 95 °C, 4 wt% catalyst, and 9:1 methanol:oleic acid molar ratio.

and magnetic separability) pave the way for simultaneous esterification and transesterification of low grade bio-oil feedstocks to biodiesel, eliminating the need for current pre-treatments to reduce the FFA content, and enabling facile and energy efficient product separation. The SO_4/Mg-Al-Fe_3O_4 catalyst exhibited good activity for biodiesel production from WCO for a 9:1 methanol:oil molar ratio and 4 wt% catalyst loading after 5 h reaction at 95 °C. It also exhibited good activity for oleic acid esterification (87% yield in 2 h) under similar reaction conditions, highlighting the potential of SO_4/Mg-Al-Fe_3O_4 for the direct conversion of low grade oil feedstocks high in FFAs to biodiesel, without requiring any pre-treatment. SO_4/Mg-Al-Fe_3O_4 demonstrates excellent stability and recyclability over five consecutive transesterification reactions with negligible deactivation or leaching, paving the way to commercial biodiesel production from WCO using a heterogeneous catalyst. Future study could involve investigation of the effect of different calcination temperatures on the catalytic performance of this magnetic catalyst. An extended study should also focus on the investigation of mechanism of this catalyst for esterification and transesterification reactions. Tests of different chain length of fatty acid composition feedstocks need to be carried out in order to better understand its effect on the performance of this type of catalyst as WCO is a mixture of different fatty acids.

Table 2
Elemental analysis of biodiesel after magnetic catalyst separation.

		Leachate concentration[a] / μg l^{-1}			
		Mg	Al	S	Fe
Spent catalyst	Run 1	0.343	0.124	0.000	0.082
	Run 2	0.308	0.098	0.000	0.028
	Run 3	0.356	0.378	0.000	0.229
	Run 4	0.327	0.120	0.000	0.067
	Run 5	0.220	0.082	0.000	0.053

[a] ICP-MS.

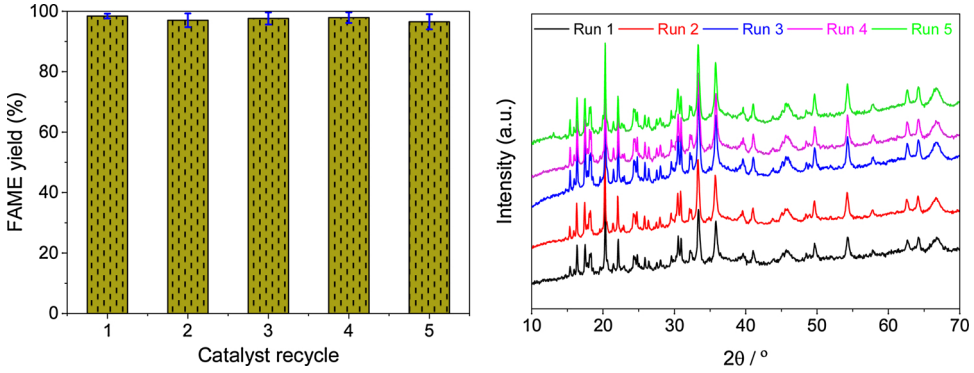

Fig. 8. (left) Transesterification of WCO over SO_4/Mg-Al-Fe_3O_4 as a function of re-use: reaction conditions: 4 wt%, 95 °C, 9:1 methanol:WCO molar ratio. (right) XRD patterns of post-reaction SO_4/Mg-Al-Fe_3O_4.

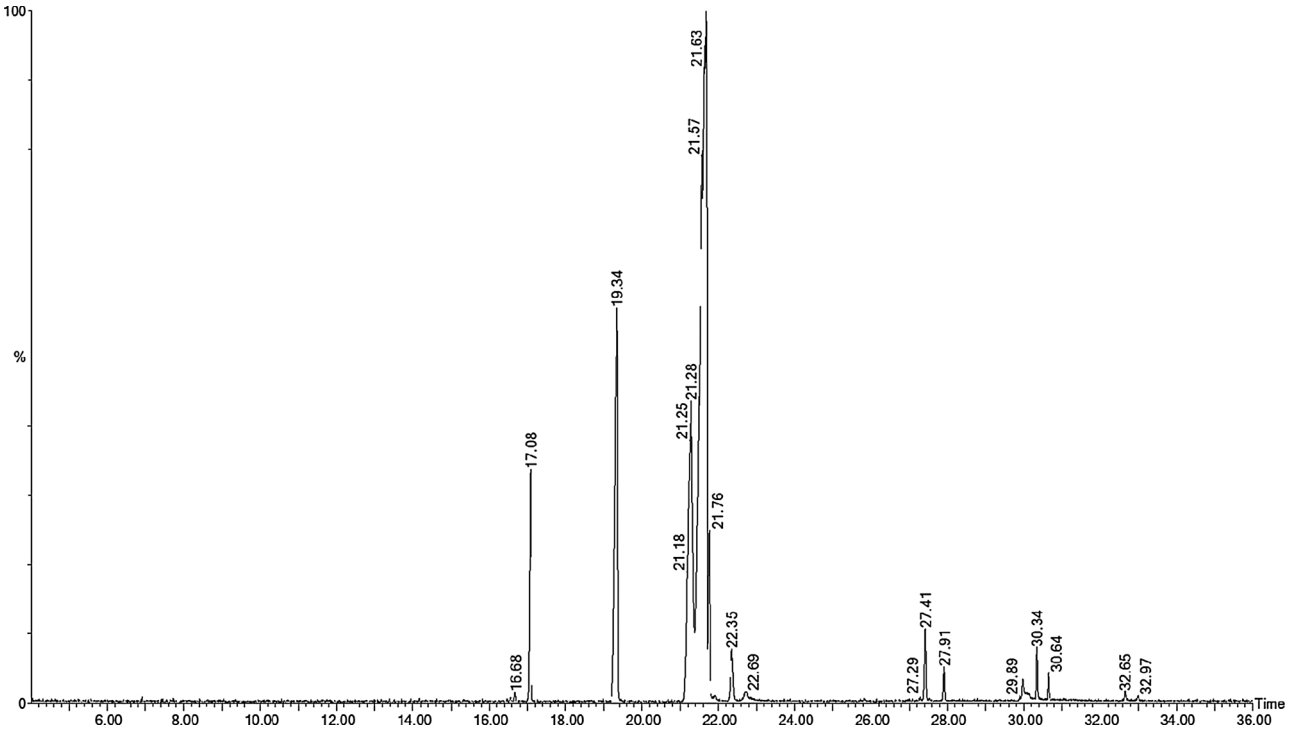

Fig. 9. GC–MS chromatogram for biodiesel product from WCO transesterification over SO_4/Mg-Al-Fe_3O_4. Reaction conditions: 4 wt% catalyst mass to WCO, 95 °C, 9:1 methanol:WCO molar ratio.

Table 3
FAME composition of biodiesel derived from WCO transesterification over SO_4/Mg-Al-Fe_3O_4.

FAME	Chain structure	Retention time / mins	Area	FAME / Area %
Myristic acid methyl ester	$C_{14:0}$	14.157	528458	0.04
Palmitic acid methyl ester	$C_{16:0}$	17.074	66629604	5.01
Palmitoleic acid methyl ester	$C_{16:1}$	16.673	2244707	0.17
Heptadecanoic acid methyl ester	$C_{17:0}$	19.334	195359776	IS
Stearic acid methyl ester	$C_{18:0}$	22.351	26016648	1.96
Oleic acid methyl ester	$C_{18:1}$	21.675	898642007	67.77
Linoleic acid methyl ester	$C_{18:2}$	21.280	279073632	20.99
Linolenic acid methyl ester	$C_{18:3}$	21.675	17771433	1.17
Gadoleic acid methyl ester	$C_{20:1}$	27.413	20598874	1.55
Erucic acid methyl ester	$C_{21:1}$	30.334	11479104	0.86
Behenic acid methyl ester	$C_{22:0}$	30.639	5037719	0.38
Lignoceric acid methyl ester	$C_{24:0}$	30.980	1328256	0.10

Table 4
Properties of biodiesel derived from WCO transesterification over SO_4/Mg-Al-Fe_3O_4.

Property	Unit	Limits		Synthesised biodiesel
		ASTM D6751	EN14214	
Flash point	°C	93 min.	101 min.	179.5
Kinematic viscosity	$mm^2\ s^{-1}$	1.9-6.0	3.5-5.0	4.74
Acid number	$mgKOH\ g^{-1}$	0.8 max.	0.5 max.	0.34
Density at 15 °C	$kg\ m^{-3}$	–	860-900	892.6
FAME content	% mass	–	96.5 min.	98.5
Methyl linolenate content	% mass	–	12 max.	1.17
Free glycerine content	% mass	0.02 max.	–	0.025
Total glycerine content	% mass	0.24 max.	0.25 max.	0.122
Monoglyceride content	% mass	–	0.8 max.	0.007
Diglyceride content	% mass	–	0.2 max.	0.008
Triglyceride content	% mass	–	0.2 max.	0.082

Declaration of Competing Interest

The authors declare no conflict of interest.

Acknowledgments

The authors are gratefully acknowledge the Ministry of Higher Education and Scientific Research of the Kurdistan Regional Government for funding this study under the Human Capacity Development Program (HCDP).

References

[1] A.E. Atabani, A.S. Silitonga, I.A. Badruddin, T. Mahlia, H. Masjuki, S. Mekhilef, A comprehensive review on biodiesel as an alternative energy resource and its characteristics, Renew. Sustain. Energy Rev. 16 (4) (2012) 2070–2093.
[2] K. Wilson, A.F. Lee, Rational design of heterogeneous catalysts for biodiesel synthesis, Catal. Sci. Technol. 2 (5) (2012) 884–897.
[3] J.A. Melero, L.F. Bautista, G. Morales, J. Iglesias, R. Sánchez-Vázquez, Biodiesel production from crude palm oil using sulfonic acid-modified mesostructured catalysts, Chem. Eng. J. 161 (3) (2010) 323–331.
[4] K.A. Younis, J.L. Gardy, K.S. Barzinji, Production and characterization of biodiesel

from locally sourced sesame seed oil, used cooking oil and other commercial vegetable oils in Erbil-Iraqi Kurdistan, Am. J. Appl. Chem. 2 (6) (2014) 105–111.
[5] J. Gardy, A. Osatiashtiani, O. Céspedes, A. Hassanpour, X. Lai, A.F. Lee, K. Wilson, M. Rehan, A magnetically separable SO_4/Fe-Al-TiO_2 solid acid catalyst for biodiesel production from waste cooking oil, Appl. Catal. B: Environ. 234 (2018) 268–278.
[6] J. Gardy, A. Hassanpour, X. Lai, M. Rehan, The influence of blending process on the quality of rapeseed oil-used cooking oil biodiesels, Int. Sci. J. (J. Environ. Sci.) 3 (2014) 233–240.
[7] Â. Silva, K. Wilson, A.F. Lee, V.C. dos Santos, A.C.C. Bacilla, K.M. Mantovani, S. Nakagaki, Nb_2O_5/SBA-15 catalyzed propanoic acid esterification, Appl. Catal. B: Environ. 205 (2017) 498–504.
[8] J.J. Creasey, A. Chieregato, J.C. Manayil, C.M. Parlett, K. Wilson, A.F. Lee, Alkali- and nitrate-free synthesis of highly active Mg–Al hydrotalcite-coated alumina for FAME production, Catal. Sci. Technol. 4 (3) (2014) 861–870.
[9] M. Rehan, J. Gardy, A. Demirbas, U. Rashid, W. Budzianowski, D. Pant, A. Nizami, Waste to biodiesel: a preliminary assessment for Saudi Arabia, Bioresour. Technol. 250 (2018) 17–25.
[10] F.H. Alhassan, U. Rashid, Y.H. Taufiq-Yap, Synthesis of waste cooking oil based biodiesel via ferric-manganese promoted molybdenum oxide/zirconia nanoparticle solid acid catalyst: influence of ferric and manganese dopants, J. Oleo Sci. 64 (5) (2015) 505–514.
[11] J. Nisar, R. Razaq, M. Farooq, M. Iqbal, R.A. Khan, M. Sayed, A. Shah, I. ur Rahman, Enhanced biodiesel production from Jatropha oil using calcined waste animal bones as catalyst, Renew. Energy 101 (2017) 111–119.
[12] L. Li, C. Zou, L. Zhou, L. Lin, Cucurbituril-protected $Cs_{2.5}H_{0.5}PW_{12}O_{40}$ for optimized biodiesel production from waste cooking oil, Renew. Energy 107 (2017) 14–22.
[13] A.F. Lee, Catalysing sustainable fuel and chemical synthesis, Appl. Petrochem. Res. 4 (1) (2014) 11–31.
[14] R.Z. Raia, L.S. da Silva, S.M.P. Marcucci, P.A. Arroyo, Biodiesel production from Jatropha curcas L. oil by simultaneous esterification and transesterification using sulphated zirconia, Catal. Today 289 (2017) 105–114.
[15] P. Upham, P. Thornley, J. Tomei, P. Boucher, Substitutable biodiesel feedstocks for the UK: a review of sustainability issues with reference to the UK RTFO, J. Clean. Prod. 17 (2009) S37–S45.
[16] C. Pirez, A. Lee, J.C. Manayil, C. Parlett, K. Wilson, Hydrothermal saline promoted grafting: a route to sulfonic acid SBA-15 silica with ultra-high acid site loading for biodiesel synthesis, Green Chem. 16 (10) (2014) 4506–4509.
[17] J. Montero, M. Isaacs, A. Lee, J. Lynam, K. Wilson, The surface chemistry of nanocrystalline MgO catalysts for FAME production: an in situ XPS study of H_2O, CH_3OH and CH_3OAc adsorption, Surf. Sci. 646 (2016) 170–178.
[18] A.F. Lee, K. Wilson, Recent developments in heterogeneous catalysis for the sustainable production of biodiesel, Catal. Today 242 (2015) 3–18.
[19] C. Komintarachat, S. Chuepeng, Solid acid catalyst for biodiesel production from waste used cooking oils, Ind. Eng. Chem. Res. 48 (20) (2009) 9350–9353.
[20] V.C. Eze, A.N. Phan, C. Pirez, A.P. Harvey, A.F. Lee, K. Wilson, Heterogeneous catalysis in an oscillatory baffled flow reactor, Catal. Sci. Technol. 3 (9) (2013) 2373–2379.
[21] A.F. Lee, J.A. Bennett, J.C. Manayil, K. Wilson, Heterogeneous catalysis for sustainable biodiesel production via esterification and transesterification, Chem. Soc. Rev. 43 (22) (2014) 7887–7916.
[22] Y.C. Sharma, B. Singh, J. Korstad, Advancements in solid acid catalysts for eco-friendly and economically viable synthesis of biodiesel, Biofuels Bioprod. Biorefining 5 (1) (2011) 69–92.
[23] J. Gardy, A. Hassanpour, X. Lai, M.H. Ahmed, M. Rehan, Biodiesel production from used cooking oil using a novel surface functionalised TiO_2 nano-catalyst, Appl. Catal. B: Environ. 207 (2017) 297–310.
[24] Y.M. Sani, W.M.A.W. Daud, A.A. Aziz, Activity of solid acid catalysts for biodiesel production: a critical review, Appl. Catal. A Gen. 470 (2014) 140–161.
[25] J.A. Melero, J. Iglesias, G. Morales, Heterogeneous acid catalysts for biodiesel production: current status and future challenges, Green Chem. 11 (9) (2009) 1285–1308.
[26] M.A. Farabi, M.L. Ibrahim, U. Rashid, Y.H. Taufiq-Yap, Esterification of palm fatty acid distillate using sulfonated carbon-based catalyst derived from palm kernel shell and bamboo, Energy Convers. Manage. 181 (2019) 562–570.
[27] J. Zhang, A. Motta, Y. Gao, M.M. Stalzer, M. Delferro, B. Liu, T.L. Lohr, T.J. Marks, Cationic pyridylamido adsorbate on Brønsted acidic sulfated zirconia: a molecular supported organohafnium catalyst for olefin homo-and co-polymerization, ACS Catal. (2018).
[28] J. Arfaoui, A. Ghorbel, C. Petitto, G. Delahay, Novel V_2O_5-CeO_2-TiO_2-SO_4^{2-} nanostructured aerogel catalyst for the low temperature selective catalytic reduction of NO by NH_3 in excess O_2, Appl. Catal. B: Environ. 224 (2018) 264–275.
[29] D. Xu, X. Lai, W. Guo, X. Zhang, C. Wang, P. Dai, Efficient catalytic properties of SO_4^{2-}/MxOy (M= Cu, Co, Fe) catalysts for hydrogen generation by methanolysis of sodium borohydride, Int. J. Hydrogen Energy 43 (13) (2018) 6594–6602.
[30] K. Kaur, A. Sobti, R.K. Wanchoo, A.P. Toor, Studies on glycerol conversion to tricaproin over sulfate promoted iron oxide as catalyst using response surface methodology, Chem. Eng. Res. Des. (2018).
[31] S. Li, H. Song, Y. Hu, F. Li, Y. Chen, A novel method for the synthesis of highly stable nickel-modified sulfated zirconia catalysts for n-pentane isomerization, Catal. Commun. 104 (2018) 57–61.
[32] A. Osatiashtiani, L.J. Durndell, J.C. Manayil, A.F. Lee, K. Wilson, Influence of alkyl chain length on sulfated zirconia catalysed batch and continuous esterification of carboxylic acids by light alcohols, Green Chem. 18 (20) (2016) 5529–5535.
[33] R.M. de Almeida, L.K. Noda, N.S. Goncalves, S.M. Meneghetti, M.R. Meneghetti, Transesterification reaction of vegetable oils, using superacid sulfated TiO_2–base catalysts, Appl. Catal. A Gen. 347 (1) (2008) 100–105.
[34] A.I. Rabee, G.A. Mekhemer, A. Osatiashtiani, M.A. Isaacs, A.F. Lee, K. Wilson, M.I. Zaki, Acidity-reactivity relationships in catalytic esterification over ammonium sulfate-derived sulfated zirconia, Catalysts 7 (7) (2017) 204.
[35] L.K. Noda, R.M. de Almeida, N.S. Gonçalves, L.F.D. Probst, O. Sala, *TiO*$_2$ with a high sulfate content—thermogravimetric analysis, determination of acid sites by infrared spectroscopy and catalytic activity, Catal. Today 85 (1) (2003) 69–74.
[36] A. Osatiashtiani, A.F. Lee, D.R. Brown, J.A. Melero, G. Morales, K. Wilson, Bifunctional SO_4/ZrO_2 catalysts for 5-hydroxymethylfufural (5-HMF) production from glucose, Catal. Sci. Technol. 4 (2) (2014) 333–342.
[37] F.H. Alhassan, U. Rashid, Y. Taufiq-Yap, Synthesis of waste cooking oil-based biodiesel via effectual recyclable bi-functional Fe_2O_3-MnO-SO_4^{2-}/ZrO_2 nanoparticle solid catalyst, Fuel 142 (2015) 38–45.
[38] H. Wu, Y. Liu, J. Zhang, G. Li, In situ reactive extraction of cottonseeds with methyl acetate for biodiesel production using magnetic solid acid catalysts, Bioresour. Technol. 174 (2014) 182–189.
[39] D. Guan, M. Fan, J. Wang, Y. Zhang, Q. Liu, X. Jing, Synthesis and properties of magnetic solid superacid: SO_4^{2-}/ZrO_2–B_2O_3–Fe_3O_4, Mater. Chem. Phys. 122 (1) (2010) 278–283.
[40] J. Li, X. Liang, Magnetic solid acid catalyst for biodiesel synthesis from waste oil, Energy Convers. Manage. 141 (2017) 126–132.
[41] G.T. Zillillah, Z. Li, Highly active, stable, and recyclable magnetic nano-size solid acid catalysts: efficient esterification of free fatty acid in grease to produce biodiesel, Green Chem. 14 (11) (2012) 3077–3086.
[42] W.-J. Liu, K. Tian, H. Jiang, H.-Q. Yu, Facile synthesis of highly efficient and recyclable magnetic solid acid from biomass waste, Sci. Rep. 3 (2013) 2419.
[43] Y.-T. Wang, X.-X. Yang, J. Xu, H.-L. Wang, Z.-B. Wang, L. Zhang, S.-L. Wang, J.-L. Liang, Biodiesel production from esterification of oleic acid by a sulfonated magnetic solid acid catalyst, Renew. Energy 139 (2019) 688–695.
[44] D. Lai, L. Deng, Q. Guo, Y. Fu, Hydrolysis of biomass by magnetic solid acid, Energy Environ. Sci. 4 (9) (2011) 3552–3557.
[45] J. Gardy, A. Hassanpour, X. Lai, M.H. Ahmed, Synthesis of Ti(SO_4)O solid acid nano-catalyst and its application for biodiesel production from used cooking oil, Appl. Catal. A Gen. 527 (2016) 81–95.
[46] J. Ropero-Vega, A. Aldana-Pérez, R. Gómez, M. Niño-Gómez, Sulfated titania [TiO_2/SO_4^{2-}]: a very active solid acid catalyst for the esterification of free fatty acids with ethanol, Appl. Catal. A Gen. 379 (1–2) (2010) 24–29.
[47] G.N. Shao, R. Sheikh, A. Hilonga, J.E. Lee, Y.-H. Park, H.T. Kim, Biodiesel production by sulfated mesoporous titania–silica catalysts synthesized by the sol–gel process from less expensive precursors, Chem. Eng. J. 215 (2013) 600–607.
[48] Z. Tai, M.A. Isaacs, C.M. Parlett, A.F. Lee, K. Wilson, High activity magnetic core-mesoporous shell sulfonic acid silica nanoparticles for carboxylic acid esterification, Catal. Commun. 92 (2017) 56–60.
[49] K. Saravanan, B. Tyagi, R.S. Shukla, H. Bajaj, Esterification of palmitic acid with methanol over template-assisted mesoporous sulfated zirconia solid acid catalyst, Appl. Catal. B: Environ. 172 (2015) 108–115.
[50] J.L.I.A. Gardy, Biodiesel production from used cooking oil using novel solid acid catalysts, Faculty of Engineering; School of Chemical and Process Engineering, The University of Leeds Whiterose e-theses, Leeds, UK, 2017.
[51] EN-14105, Fat and Oil Derivatives. Fatty Acid Methyl esters (FAME). Determination of Free and Total Glycerol and Mono-, Di-, Triglyceride Contents, (2011), pp. 1–26.
[52] P. Klobes, K. Meyer, R.G. Munro, Porosity and Specific Surface Area Measurements for Solid Materials, National Institute of Standards and Technology, U.S, 2006 p. 89.
[53] C. Yuan, H. Liu, X. Gao, Magnetically recoverable heterogeneous catalyst: tungstate intercalated Mg–Al-layered double hydroxides-encapsulated Fe_3O_4 nanoparticles for highly efficient selective oxidation of sulfides with H_2O_2, Catal. Letters 144 (1) (2014) 16–21.
[54] A.A. Kiss, F. Omota, A.C. Dimian, G. Rothenberg, The heterogeneous advantage: biodiesel by catalytic reactive distillation, Top. Catal. 40 (1–4) (2006) 141–150.
[55] A.I. Rabee, L.J. Durndell, N.E. Fouad, L. Frattini, M.A. Isaacs, A.F. Lee, G.A. Mekhemer, V.C. dos Santos, K. Wilson, M.I. Zaki, Citrate-mediated sol–gel synthesis of Al-substituted sulfated zirconia catalysts for α-pinene isomerization, Mol. Catal. 458 (2018) 206–212.
[56] T. Xin, M. Ma, H. Zhang, J. Gu, S. Wang, M. Liu, Q. Zhang, A facile approach for the synthesis of magnetic separable Fe_3O_4@TiO_2, core–shell nanocomposites as highly recyclable photocatalysts, Appl. Surf. Sci. 288 (2014) 51–59.
[57] H. Naeimi, Z.S. Nazifi, A highly efficient nano-Fe_3O_4 encapsulated-silica particles bearing sulfonic acid groups as a solid acid catalyst for synthesis of 1, 8-dioxo-octahydroxanthene derivatives, J. Nanoparticle Res. 15 (11) (2013) 2026.
[58] H. Naeimi, S. Mohamadabadi, Sulfonic acid-functionalized silica-coated magnetic nanoparticles as an efficient reusable catalyst for the synthesis of 1-substituted 1 H-tetrazoles under solvent-free conditions, Dalton Trans. 43 (34) (2014) 12967–12973.
[59] S. Gadamsetti, N. Mathangi, S. Hussain, V.K. Velisoju, K.V. Chary, Vapor phase esterification of levulinic acid catalyzed by γ-Al_2O_3 supported molybdenum phosphate catalysts, Mol. Catal. (2018).
[60] W. Sheng, W. Wei, J. Li, X. Qi, G. Zuo, Q. Chen, X. Pan, W. Dong, Amine-functionalized magnetic mesoporous silica nanoparticles for DNA separation, Appl. Surf. Sci. 387 (2016) 1116–1124.
[61] S. Sen, V. Govindarajan, C.J. Pelliccione, J. Wang, D.J. Miller, E.V. Timofeeva, Surface modification approach to TiO_2 nanofluids with high particle concentration, low viscosity, and electrochemical activity, ACS Appl. Mater. Interfaces 7 (37) (2015) 20538–20547.
[62] J. Wang, P. Yang, M. Fan, W. Yu, X. Jing, M. Zhang, X. Duan, Preparation and characterization of novel magnetic ZrO_2/TiO_2/Fe_3O_4 solid superacid, Mater. Lett. 61 (11–12) (2007) 2235–2238.
[63] H. Zhao, P. Jiang, Y. Dong, M. Huang, B. Liu, A high-surface-area mesoporous

sulfated nano-titania solid superacid catalyst with exposed (101) facets for esterification: facile preparation and catalytic performance, New J. Chem. 38 (9) (2014) 4541–4548.

[64] S.S. Vieira, Z.M. Magriotis, N.A. Santos, A.A. Saczk, C.E. Hori, P.A. Arroyo, Biodiesel production by free fatty acid esterification using lanthanum (La^{3+}) and HZSM-5 based catalysts, Bioresour. Technol. 133 (2013) 248–255.

[65] F. Jamil, H. Ala'a, M.T.Z. Myint, M. Al-Hinai, L. Al-Haj, M. Baawain, M. Al-Abri, G. Kumar, A. Atabani, Biodiesel production by valorizing waste Phoenix dactylifera L. Kernel oil in the presence of synthesized heterogeneous metallic oxide catalyst (Mn@ MgO-ZrO_2), Energy Convers. Manage. 155 (2018) 128–137.

[66] Z. Zhang, H. Huang, X. Ma, G. Li, Y. Wang, G. Sun, Y. Teng, R. Yan, N. Zhang, A. Li, Production of diacylglycerols by esterification of oleic acid with glycerol catalyzed by diatomite loaded SO_4^{2-}/TiO_2, J. Ind. Eng. Chem. 53 (2017) 307–316.